The Orientation of Eosin-5-Maleimide on Human Erythrocyte Band 3 Measured by Fluorescence Polarization Microscopy

Scott M. Blackman, Charles E. Cobb, Albert H. Beth, and David W. Piston
Department of Molecular Physiology and Biophysics, Vanderbilt University, Nashville, Tennessee 37232 USA

ABSTRACT The dominant motional mode for membrane proteins is uniaxial rotational diffusion about the membrane normal axis, and investigations of their rotational dynamics can yield insight into both the oligomeric state of the protein and its interactions with other proteins such as the cytoskeleton. However, results from the spectroscopic methods used to study these dynamics are dependent on the orientation of the probe relative to the axis of motion. We have employed polarized fluorescence confocal microscopy to measure the orientation of eosin-5-maleimide covalently reacted with Lys-430 of human erythrocyte band 3. Steady-state polarized fluorescence images showed distinct intensity patterns, which were fit to an orientation distribution of the eosin absorption and emission dipoles relative to the membrane normal axis. This orientation was found to be unchanged by trypsin treatment, which cleaves band 3 between the integral membrane domain and the cytoskeleton-attached domain. This result suggests that phosphorescence anisotropy changes observed after trypsin treatment are due to a rotational constraint change rather than a reorientation of eosin. By coupling time-resolved prompt fluorescence anisotropy with confocal microscopy, we calculated the expected amplitudes of the e^{-Dt} and e^{-4Dt} terms from the uniaxial rotational diffusion model and found that the e^{-4Dt} term should dominate the anisotropy decay. Delayed fluorescence and phosphorescence anisotropy decays of control and trypsin-treated band 3 in ghosts, analyzed as multiple uniaxially rotating populations using the amplitudes predicted by confocal microscopy, were consistent with three motional species with uniaxial correlation times ranging from 7 μs to 1.4 ms.

INTRODUCTION

The erythrocyte anion exchange protein, band 3, is the major integral membrane protein of the red cell, comprising 25–30% of the total membrane protein by weight (Fairbanks et al., 1971). Band 3 consists of two structurally and functionally distinct domains: a ~55-kDa carboxy-terminal transmembrane portion, and a ~43-kDa amino-terminal cytoplasmic portion (Tanner et al., 1988; Lux et al., 1989). The transmembrane domain of band 3 traverses the membrane an even number of times (probably 10–14; Lieberman and Reithmeier, 1988) and is sufficient to catalyze the electroneutral exchange of bicarbonate and chloride anions (Lepke and Passow, 1976). The water-soluble cytoplasmic domain does not have a strong association with the plasma membrane; however, it contains binding sites for components of the erythrocyte cytoskeleton (ankyrin and band 4.2) as well as a number of other cytosolic proteins (reviewed in Low, 1986). A substantial body of literature has provided strong support for the importance of an intact cytoskeleton, maintenance of its normal interaction with intrinsic membrane proteins including band 3, and the proper flexibility of these proteins, for the erythrocyte membrane to exhibit normal shape and mechanical properties (see Palek and Lambert, 1990, and Wang, 1994, for reviews).

Received for publication 16 January 1996 and in final form 5 April 1996.
Address reprint requests to Dr. Albert H. Beth or Dr. David W. Piston, Department of Molecular Physiology and Biophysics, 702 Light Hall, Vanderbilt University, Nashville, TN 37232. Tel.: 615-322-7030; Fax: 615-322-7236; E-mail: beth@lhmrba.hh.vanderbilt.edu or dave.piston@mcmail.vanderbilt.edu.

0006-3495/96/07/194/15 $2.00

The global rotational dynamics of band 3 are expected to be sensitive to the band 3-cytoskeleton interaction and to the oligomeric state of band 3. The simplest model for the rotational dynamics of integral membrane proteins is the uniaxial rotational diffusion (URD) model (Saffman and Delbrück, 1975; Jähnig, 1986), which approximates the protein as a cylinder undergoing rotational diffusion about a single axis, the membrane normal axis. One determinant of the rate of this motion is the radius of the intramembrane portion of the protein, which should be affected by the formation of oligomers of band 3. Furthermore, association of band 3 with the cytoskeleton may restrict the amplitude of rotational excursions from an equilibrium position (compared to the freely rotating untethered state) or may promote interactions with itself or other proteins.

Because of the high viscosity of the lipid bilayer, spectroscopic techniques for measuring the global rotational motions of membrane proteins must be sensitive to dynamics on the microsecond to millisecond time scale. Techniques used to measure band 3 rotational dynamics have included saturation-transfer electron paramagnetic resonance (ST-EPR) (Beth et al., 1986; Hustedt and Beth, 1995; reviewed in Thomas, 1985, 1986) and a variety of time-resolved triplet-state optical techniques, including transient linear dichroism (e.g., Cherry et al., 1976; Nigg and Cherry, 1980), delayed fluorescence or phosphorescence anisotropy (Tsuji et al., 1988; Matayoshi and Jovin, 1991, Matayoshi et al., 1991; McPherson et al., 1992, 1993; Corbett and Golan, 1993), and fluorescence recovery spectroscopy (Johnson and Garland, 1981). The best characterized fluorescent/phosphorescent probe for band 3 is eosin-5-maleimide (EMA), which has been shown to react covalently with band

3 at a single amino acid, Lys-430, and compete with the stilbenedisulfonate class of anion transport inhibitors at approximately 1:1 stoichiometry (Cobb and Beth, 1990).

Although the rotational dynamics of band 3 have been of considerable interest, the optical spectroscopic data remain difficult to interpret. Anisotropy decay data indicate multiple motional processes occurring over periods of microseconds to milliseconds, which has been suggested to mean that most of band 3 is aggregated to some degree (e.g., Matayoshi and Jovin, 1991). It has been difficult to assign these multiple decay components in the data to actual molecular species, which would be consistent with the large body of biochemical data on band 3. The URD model predicts two exponential decay components for each molecular species, and that the anisotropy at long times (r_∞) is generally nonzero. The amplitudes of the two decay components and r_∞ depend on the orientation of the chromophore with respect to the diffusion axis. Independent measurement of the orientation of the EMA chromophore on band 3 would provide a powerful constraint to test which of the multiple decay modes is consistent with a species undergoing uniaxial rotational diffusion (e.g., Heyn et al., 1977; Cherry and Godfrey, 1981; Lin and Mathies, 1989). Although the orientation of EMA on band 3 has not been determined previously, the average angle between its absorption dipole and the diffusion axis has been estimated from transient dichroism decay curves (Morrison et al., 1986). Additionally, to interpret emission anisotropy decays such as delayed fluorescence, information about the fluorescence emission dipole orientation is required.

Recent EPR studies by Hustedt and Beth (1996) have indicated that the major rotational diffusion axis of band 3, as reported by a spin-labeled stilbenedisulfonate, is coincident with the membrane normal axis. Therefore, as a starting point for a more detailed investigation of the multiexponential anisotropy decays of band 3, a valid assumption would be that the orientation of eosin relative to the diffusion axis is equivalent to its orientation relative to the membrane normal axis. This orientation distribution may be measured by angle-resolved fluorescence spectroscopy on macroscopically oriented systems such as muscle fibers (e.g., Van der Heide et al., 1994; Burghardt and Ajtai, 1994), planar bilayers (e.g., Zannoni et al., 1983), or cell membranes in a microscope field (e.g., Axelrod, 1979; Florine-Casteel, 1990). In this work, we report the measurement of the orientation distribution of the absorption and fluorescence emission dipoles of eosin-5-maleimide on band 3, by analysis of microscopic images of individual erythrocyte ghosts. This represents the first measurement of the orientation of EMA-labeled band 3 in erythrocyte ghosts, the system in which most previous spectroscopic experiments on band 3 have been performed. This result has enabled prediction of the two preexponential amplitudes and r_∞ of the URD model. Although the source of the multiple anisotropy decay components for band 3 is unknown, time-resolved delayed fluorescence and phosphorescence anisotropy data were analyzed under the assumption that all decays arise from uniaxially rotating species, using the preexponential amplitudes predicted from the microscopy data. The fastest rotating populations had uniaxial rotational diffusion constants consistent with reasonable estimates for a freely rotating band 3 dimer or tetramer. Portions of this work have been published as abstracts (Blackman et al., 1995, 1996).

THEORY

A theoretical model has been developed to describe the orientation-dependent, steady-state fluorescence signal, as a function of the chromophore orientation, in the confocal microscope field. The chromophore orientation is represented by two order parameters ($\langle P_2(\cos\theta_a)\rangle$ and $\langle P_2(\cos\theta_e)\rangle$) and three correlation functions, C_0, C_1, and C_2, which correspond in the URD model to the residual anisotropy and the amplitudes of the e^{-Dt} and e^{-4Dt} exponential decay terms, respectively. There is a large body of theoretical modeling and experimental data describing fluorescence in oriented systems, using different experimental geometries (e.g., Van der Meer et al., 1982; Zannoni et al., 1983; Van der Heide et al., 1994; Burghardt and Ajtai, 1994). Whereas some similar approaches have expanded C_0, C_1, and C_2 in terms of orientational order parameters (e.g., Van der Meer et al., 1982), we are primarily interested in these correlation functions because of their appearance in the URD model. Therefore, the goal of this section is to obtain the numerical values of $C_0(\infty)$, $C_1(\infty)$, and $C_2(\infty)$, leaving implicit their dependence on orientational order parameters.

Orientation-dependent fluorescence intensities

For a polarized excitation pulse at $t = 0$, three intensity functions I_x, I_y, I_z are defined by

$$I_{[x,y,z]}(t) = S(t)\langle(\mathbf{l}\cdot\mathbf{a}(0))^2(\mathbf{e}(t)\cdot\mathbf{p})^2\rangle = S(t)\langle\cos^2\theta_{la}\cos^2\theta_{ep}\rangle, \quad (1)$$

where $S(t)$ is proportional to the total intensity of emission, $\mathbf{a}(0)$ and $\mathbf{e}(t)$ are the absorption and emission dipole vectors at times 0 and t, respectively, $\mathbf{l}$ is the laser polarization vector (laboratory $\times$ axis), $\mathbf{p}$ is the emission polarizer direction vector (X, Y, or Z directions), and θ_{la} and θ_{ep} denote the angles between the subscripted vectors. The brackets denote an ensemble average over all fluorophores within a given pixel. Here and below, the time dependence is implicit: all absorption processes occur at time 0, and emission at time t. The high numerical aperture (NA) of the confocal microscope requires the use of correction factors (Axelrod, 1979), and the observed intensities for emission polarizer parallel and perpendicular to the laser polarization are given by

$$I_\parallel = K_c I_x + K_b I_y + K_a I_z \qquad I_\perp = K_b I_x + K_c I_y + K_a I_z, \quad (2)$$

where the microscope optical axis is Z. In the limit of zero NA, $K_c = 1$, and $K_a = K_b = 0$. Using an expression similar to equation 18 of Florine-Casteel (1990), it is also straightforward to extend this model to arbitrary emission polarizer orientations.

Following the general outline of Van der Meer et al. (1982), Eq. 1 is rewritten using the Wigner rotation matrix elements (Edmonds, 1960), using the relation to the Legendre polynomials: $D^2_{00}(\alpha\ \beta\ \gamma) = P_2(\cos\beta) = \frac{1}{2}(3\cos^2\beta - 1)$:

$$\begin{aligned} 9\,I_{[x,y,z]} &= S(t)\langle(1 + 2D^2_{00}(\Omega_{la}))(1 + 2D^2_{00}(\Omega_{ep}))\rangle \\ &= S(t)\{1 + 2\langle D^2_{00}(\Omega_{la})\rangle + 2\langle D^2_{00}(\Omega_{ep})\rangle \\ &\quad + 4\langle D^2_{00}(\Omega_{la})D^2_{00}(\Omega_{ep})\rangle\}, \end{aligned} \tag{3}$$

where Ω_{la} denotes the set of Euler angles that rotate the laser polarization vector into the absorption dipole, and Ω_{ep} rotate the emission dipole into the polarizer direction. This expression consists of two time-independent order parameters, and a correlation function that contains information about the dynamics as well as the orientation distribution.

To separate macroscopic (known) parameters from microscopic (unknown) parameters, these two Euler rotations are decomposed into three successive rotations (see Fig. 1, *A* and *B*): from the laser polarization direction (X axis) to the laboratory Z axis ($\Omega_{lZ} = (0\ \pi/2\ 0)$), from the laboratory Z axis to the membrane normal vector ($\Omega_{ZN} = (0\ \alpha\ \pi/2\ -\beta)$), and from the membrane normal to the absorption dipole ($\Omega_{Na} = (0\ \theta_a\ \eta)$). Ω_{ep} is decomposed similarly to get $\Omega_{eN} = -\Omega_{Ne} = (-(\eta + \psi)\ -\theta_e\ 0)$. Furthermore, because **p** can represent the laboratory X, Y, or Z axis, rotations between laboratory axes are used: $\Omega_{ZX} = (0\ -\pi/2\ 0)$, $\Omega_{ZY} = (0\ -\pi/2\ -\pi/2)$. Using the closure relation of Wigner rotation matrices, one obtains

$$D^2_{00}(\Omega_{la}) = \sum_{j,k} D^2_{0j}(\Omega_{lZ})D^2_{jk}(\Omega_{ZN})D^2_{k0}(\Omega_{Na}). \tag{4}$$

$$D^2_{00}(\Omega_{ep}) = \sum_{j,k} D^2_{0j}(\Omega_{eN})D^2_{jk}(\Omega_{NZ})D^2_{k0}(\Omega_{Zp}). \tag{5}$$

Because the membrane is a cylindrically symmetric system, all expressions are averaged over one period of η, which denotes rotation around the membrane normal axis (see Fig. 1 *B*). After substitution and simplification, one obtains

$$\begin{aligned} 9\,I_{[x,y,z]} &= S(t)\{1 + Q_0\langle d^2_{00}(\theta_a)\rangle + R_0\langle d^2_{00}(\theta_e)\rangle \\ &\quad + \sum_k Q_k R_k\langle d^2_{k0}(\theta_a)d^2_{0k}(-\theta_e)\exp(-ik\phi)\rangle\}, \end{aligned} \tag{6}$$

where Q_k and R_k are functions of the (known) angles α and β:

$$Q_k = \sum_{j=-2}^{2} D^2_{kj}(\Omega_{lZ})D^2_{j0}(\Omega_{ZN}) \tag{7a}$$

$$R_k = \sum_{j=-2}^{2} D^2_{kj}(\Omega_{NZ})D^2_{j0}(\Omega_{Zp}). \tag{7b}$$

Rearrangement of the summation in Eq. 6, noting that $Q_{-k}R_{-k} = Q_kR_k^*$, allows the five complex correlation functions to be rewritten as five real correlation functions.

In this work, experimental data are confined to a thin optical cross section through the equator of the ghost membrane. This is simulated by averaging α from $\alpha = \pi/2 - \delta$ to $\pi/2 + \delta$, where δ is a small angle related to the slice thickness (see Fig. 1 *A*). In this experimental geometry, only three of the five correlation functions contribute to the final expressions

$$\begin{aligned} C_0(t) &= \frac{2}{5}\langle d^2_{00}(\theta_a)d^2_{00}(\theta_e)\rangle \\ C_1(t) &= \frac{4}{5}\langle d^2_{10}(\theta_a)d^2_{01}(\theta_e)\cos\Psi\rangle \\ C_2(t) &= \frac{4}{5}\langle d^2_{20}(\theta_a)d^2_{02}(\theta_e)\cos 2\Psi\rangle, \end{aligned} \tag{8}$$

where the correlation functions have been normalized according to their contribution to the anisotropy in isotropic solution (see Eq. 14, below). Finally, the steady-state fluorescence intensity is obtained by integrating the expressions according to

$$\bar{I}_{[x,y,z]} = \int_0^\infty I_{[x,y,z]}(t)\,dt \Big/ \int_0^\infty S(t)\,dt, \tag{9}$$

which yields equations in which $C_0(t)$, $C_1(t)$, $C_2(t)$ have been replaced by time-averaged counterparts $\bar{C}_0$, $\bar{C}_1$, $\bar{C}_2$,

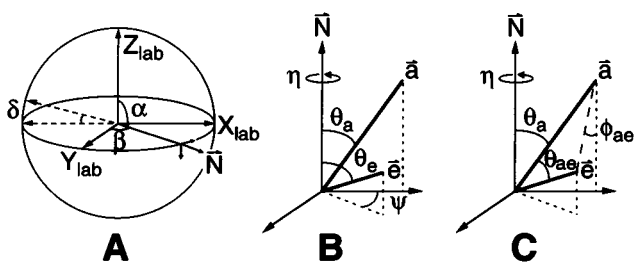

FIGURE 1 Definitions of angles used in this study. (*A*) Angles α and β, which define the orientation of the membrane normal with respect to the laboratory axes X, Y, Z. δ is the half-angle over which the membrane angle α is averaged due to finite slice thickness. The small axis system on the surface represents the membrane reference frame, shown in detail in *B*. (*B*) Parameterization used in model A. N is the membrane normal axis, a and e are the absorption and emission dipole vectors, η represents a rotation around N, θ_a and θ_e are the angles between N and the absorption and emission dipoles, and ψ is a rotation of e around N. (*C*) The parameterization used in model B. θ_{ae} is the interdipole angle, and ϕ_{ae} is a rotation of e around a.

defined by expressions similar to Eq. 9. No assumptions are made here about the form of the $S(t)$ decay. For the limiting case of $\delta = 0$ (negligible optical section thickness), orientation-dependent intensities are given by

$$\bar{I}_x \propto 1 + 10\bar{C}_0 + 2\langle P_2(\cos\theta_a)\rangle + 2\langle P_2(\cos\theta_e)\rangle + \cos^2\beta(-30\bar{C}_0 + 15\bar{C}_1 - 3\langle P_2(\cos\theta_a)\rangle - 3\langle P_2(\cos\theta_e)\rangle) + \cos^4\beta\left(\frac{45}{2}\bar{C}_0 - 15\bar{C}_1 + \frac{15}{4}\bar{C}_2\right) \quad (10)$$

$$\bar{I}_y \propto 1 - 5\bar{C}_0 + 2\langle P_2(\cos\theta_a)\rangle - \langle P_2(\cos\theta_e)\rangle + \cos^2\beta\left(\frac{45}{2}\bar{C}_0 - 15\bar{C}_1 + \frac{15}{4}\bar{C}_2 - 3\langle P_2(\cos\theta_a)\rangle + 3\langle P_2(\cos\theta_e)\rangle\right) + \cos^4\beta\left(-\frac{45}{2}\bar{C}_0 + 15\bar{C}_1 - \frac{15}{4}\bar{C}_2\right) \quad (11)$$

$$\bar{I}_z \propto 1 - 5\bar{C}_0 + 2\langle P_2(\cos\theta_a)\rangle - \langle P_2(\cos\theta_e)\rangle + \cos^2\beta\left(\frac{15}{2}\bar{C}_0 - \frac{15}{4}\bar{C}_2 - 3\langle P_2(\cos\theta_a)\rangle\right), \quad (12)$$

where the notation $\langle d^2_{00}(\theta)\rangle$ has been replaced by its equivalent, $\langle P_2(\cos\theta)\rangle$. The derivations leading to Eqs. 10–12 will be referred to as model A.

We define model B as an extension to model A, in which a functional form for the orientation distribution is assumed, and the five parameters of model A are calculated from that distribution (e.g., equation 1 in Van der Meer et al., 1982). The functional form used below is a Gaussian distribution, the five parameters of which are θ_a, ϕ_{ae}, their standard deviations $\Delta\theta_a$ and $\Delta\phi_{ae}$, and the interdipole angle θ_{ae} (see Fig. 1 *C*). Shown in Fig. 2 are simulated fluorescence intensity profiles for chromophore dipoles oriented parallel ($\theta_a = \theta_e = 0°$) and perpendicular ($\theta_a = \theta_e = 90°$) to the membrane normal axis.

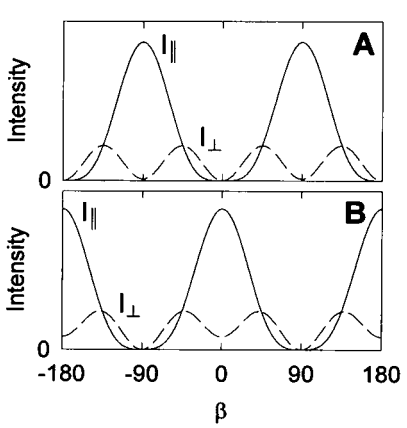

FIGURE 2 Simulated orientation-dependent intensities for immobile fluorophores oriented parallel (*A*) and perpendicular (*B*) to the membrane normal axis. Curves were simulated using co-linear absorption and emission dipoles, whose angles to the membrane normal axis were 0° and 90°, respectively. Parameters were (*A*) $P_2(\cos\theta_a) = 1$, $P_2(\cos\theta_e) = 1$, $C_0 = 1$, $C_1 = 0$, $C_2 = 0$; and (*B*) $P_2(\cos\theta_a) = -0.5$, $P_2(\cos\theta_e) = -0.5$, $C_0 = 1$, $C_1 = 0$, $C_2 = 1$.

By averaging over the angles α and β, Eq. 6 simplifies to an expression for the anisotropy (r) in an isotropic sample (equivalent to equation 8 in Van der Heide et al., 1994):

$$\tilde{I}_{[x,y,z]}(t) = \frac{1}{4\pi}\int\int I_{[x,y,z]}(t)\sin\alpha\, d\alpha\, d\beta \quad (13)$$

$$r(t) = \frac{\tilde{I}_x(t) - \tilde{I}_y(t)}{\tilde{I}_x(t) + \tilde{I}_y(t) + \tilde{I}_z(t)} = C_0(t) + C_1(t) + C_2(t), \quad (14)$$

noting that $\tilde{I}_y$ is equal to $\tilde{I}_z$. By using this, a measurement of fluorescence anisotropy (steady-state or time-resolved) from an isotropic sample may be related to C_0, C_1, and C_2.

Connection to global uniaxial rotational diffusion

The expression for the delayed fluorescence/phosphorescence anisotropy according to the URD model is a simplification of a model describing rotational diffusion of an ellipsoid (Rigler and Ehrenberg, 1973; equation 3.7 in Szabo, 1984), after setting $D_\perp = 0$:

$$r(t) = \frac{2}{5}\sum_{k=-2}^{2}\langle D^2_{k0}(\Omega_{Ne})D^2_{0k}(\Omega_{aN})\rangle\exp(-k^2D_\parallel t) = \sum_{k=0}^{2} C_k(t)\exp(-k^2D_\parallel t), \quad (15)$$

where $D_\parallel$ is the rate constant for URD, and the expressions for $C_k(t)$ are given by Eq. 8. Because prompt and delayed fluorescence utilize the same absorption and emission dipoles, the orientation parameters determined by confocal microscopy can be used to constrain the delayed fluorescence anisotropy measurements. To do this, two methods have been used to calculate values for the two preexponential amplitudes and the r_∞ of the URD model. For both, it is necessary to make the assumption that the global rotational diffusion is dominated by motions about the membrane normal axis, which are much slower than the independent probe motions. In this case, the URD amplitudes are given by $C_k(\infty)$. The first method assumes that all significant independent probe motion occurs on the prompt fluorescence time scale (~12 ns). The residual anisotropy observed in time-resolved prompt fluorescence is used as the initial delayed fluorescence anisotropy, which equals $C_0(\infty) + C_1(\infty) + C_2(\infty)$, according to Eq. 14. The $C_0(\infty)$ term is determined by the two order parameters of model A:

$$C_0(\infty) = r_\infty = \frac{2}{5}\langle P_2(\cos\theta_a)\rangle\langle P_2(\cos\theta_e)\rangle. \quad (16)$$

Although this method provides no insight into the relative amplitudes of $C_1(\infty)$ and $C_2(\infty)$, as a starting point in this study, their ratio is approximated by the ratio $\bar{C}_2/\bar{C}_1$, which

determines all three $C_k(\infty)$. The second method makes the approximation that the true orientation distribution is reasonably modeled by a Gaussian distribution, and calculates the three $C_k(\infty)$ using the parameters of model B. By using this combination of confocal microscopy and time-resolved fluorescence anisotropy, all three preexponential amplitude parameters may be fixed in the analysis of delayed fluorescence anisotropy data.

MATERIALS AND METHODS

Preparation of labeled erythrocyte ghosts

Experimental protocols followed those of Cobb and Beth (1990), except that 113 mM sodium citrate, pH 7.4 (113cit7.4), was substituted for phosphate-buffered saline. Briefly, fresh whole human blood was drawn into heparinized Vacutainer tubes and washed in ice-cold citrate buffer (suspended, centrifuged, and supernatant aspirated). Unsealed ghost membranes were prepared by hypotonic lysis in 20 volumes of 5 mM phosphate, pH 7.4 (5P7.4). When overnight storage was necessary, ghosts were purged with nitrogen gas and stored at 4°. Trypsin treatment of ghosts was performed with 5 μg/ml trypsin (12,600 U/mg; Sigma, St. Louis, MO) for 30 min on ice and was verified to be greater than 90% by gel electrophoresis (Laemmli, 1970). The treated ghost membranes were washed once with 30 μg/ml phenylmethylsulfonyl fluoride in 5P7.4, then washed three times with 5P7.4.

Labeling of intact erythrocytes with eosin-5-maleimide (Molecular Probes, Eugene, OR) was performed according to the method of Cobb and Beth (1990). For preblocking, packed erythrocytes were incubated with 100 μM H_2DIDS (4,4′-diisothiocyanatodihydrostilbene-2,2′-disulfonate; Molecular Probes), 1 h at 37°C; unreacted H_2DIDS was removed using the same procedures for removing free EMA (wash with 0.2% bovine serum albumin in 113cit7.4, then 113cit7.4). For labeling with DiI (1,1′-dioctadecyl-3, 3,3′,3′-tetramethylindocarbocyanine perchlorate; Molecular Probes), a 1.25 mg/ml ethanol solution of DiI was slowly injected into citrate buffer to 2.5 or 5 μg/ml final concentration. For each label, one drop of erythrocytes (diluted 1:1 in 113cit7.4) was added to 0.5 ml of the solution of DiI vesicles. After 5 min, 0.5 ml citrate was added, and the cells were pelleted and washed once more.

Confocal microscopy

A Zeiss LSM 410 confocal microscope, with a 40×, N.A. 1.3 Plan-Neofluar oil-immersion objective, was used to collect all image data. Excitation was at 488 nm using a standard fluorescein filter set, which provided off-peak excitation of eosin samples, but allowed efficient emission collection through a long-pass (>515 nm) filter. Both excitation and emission passed through film polarizers, and when needed, a half-wave plate was used to rotate the excitation polarization 90°. Vertical and horizontal positions of the excitation and emission polarizers are abbreviated as vv, vh, hv, and hh; parallel positions are hh and vv and perpendicular positions are vh and hv. Excitation polarization, measured by reflection confocal microscopy of a highly scattering sample, was greater than 500:1. The inherent vertical/horizontal detection bias of the apparatus (g-factor) was measured using four images (polarizer orientations vv, vh, hv, hh) of deep-well solution samples of varying viscosity. The g-factor was calculated from the equation $vv/(g \cdot vh) = (g \cdot hh)/hv$, derived from the end-on detection geometry of the microscope. Because the g-factor was found to be emission wavelength dependent, the value was confirmed using images of individual labeled erythrocyte ghosts. The thickness of confocal optical slices at the experimental pinhole setting was determined by measuring the point-spread function of 0.1-μm gold beads (Sandison et al., 1994, 1995), which had a full width at half-maximum (FWHM) of 0.7 μm along the optical axis. Using the average cell diameter of 6.4 μm, this corresponds to a half-angle of $\delta = 6°$ (see Fig. 1 *A*). Because out-of-focus fluorophores are not all located along the optical axis, the effective FWHM is probably slightly greater (δ was set to 9° for this work), but fit results were not significantly altered by using values of δ up to 15°. The lateral FWHM (determined from the same point-spread function) was 0.2 μm, and the pixel size (0.2083 μm) was chosen to match the resolution limit. All data were taken within the dynamic range of the instrument, measured by the method of Dix and Verkman (1990), and absolute numbers of photons were determined following the method of Sandison et al. (1995).

Ghost samples for microscopy were diluted 1:10 in 5P7.4 (approximately 0.25 mg/ml total protein concentration). For 10°C and 34°C experiments, the sample temperature was controlled by running coolant from a refrigeration/heating unit through the microscope stage. The amount of background labeling was determined by quantitating emission from ghosts that were treated with H_2DIDS before EMA labeling, and was less than 2%.

Images were obtained of spatially isolated, approximately circular EMA-labeled ghosts, with the confocal slice positioned at the ghost equator. Irreversible photobleaching (10–15% per scan) was observed at the experimental settings (15 μs exposure time per pixel). To correct for photobleaching, a series of image pairs (with the emission polarizer parallel or perpendicular to the excitation) was obtained for each field of ghosts. The average intensity for each ghost was fit to an exponential decay (using different initial values for parallel and perpendicular, but the same decay constant), and the pixel values were corrected before analysis. Equivalent numbers of ghosts were imaged, starting with the polarizer parallel and perpendicular. Only the first image pair of the bleach series was used for further analysis.

Image analysis

In each microscope field, one to five spatially isolated ghosts were selected for analysis. The ghost border was defined by an ellipse that maximized the pixel intensities on its boundary. The ellipse was described by five parameters (center coordinates, major and minor axes, rotation), which were optimized by using a downhill simplex algorithm (Press et al., 1992). All selected ghosts were ellipsoid, with an average diameter of 6.4 ± 0.7 μm and an average eccentricity of 0.36. The most eccentric ghost used was 0.69 (corresponding to a major:minor axis ratio of 1.9:1), the data of which overlaid those from more circular ghosts. For each pixel on the ellipse, a membrane tilt angle (β) was calculated from the ellipse parameters. Data from multiple ghosts were fit simultaneously without signal averaging to the theoretical models developed here, using a set of Marquardt-Levenberg least-squares analysis routines (Beechem et al., 1991; Beechem, 1992; Bevington, 1969). To account for unknown contributions to the signal amplitude (laser power at the sample, dye concentration, etc.), simulations were multiplied by a constant factor (not required to be the same for each ghost) determined by linear least-squares. Rigorous confidence intervals were generated by fixing the parameter of interest and allowing minimization to proceed over the remaining parameters.

Fluorescence spectroscopy

Time-resolved fluorescence anisotropy measurements were obtained using a time-resolved fluorimeter described elsewhere (Cobb et al., 1993). For this work, excitation was 568 nm, and the emission monochrometer was set to 610 nm. Ghost samples exhibited a fast (100 ps) scattering component, which was measured on turbidity-matched unlabeled ghosts and subtracted during data analysis. Anisotropy (r) and total intensity (S) were calculated as described by Cobb et al. (1993). Total intensity and anisotropy data were simultaneously fit by using a Marquardt-Levenberg global analysis package (Beechem et al., 1991; Beechem, 1992; Bevington, 1969) to an empirical model containing multiple exponential decay components:

$$r(t) = r_\infty + \sum_{i=1}^{n} \beta_i \exp(-t/\phi_i). \qquad (17)$$

To compare time-resolved anisotropy data (excitation 568 nm) with confocal microscope and delayed fluorescence data (excitation 488 and 523 nm), the ratio of steady-state anisotropy values (taken at all three wavelengths) was used as an approximate correction factor to account for the changing absorption dipole position (Van der Heide et al., 1992). Steady-state fluorescence anisotropy measurements of EMA-labeled ghosts were performed on a SPEX 1681 Fluorolog spectrometer with a 250-W xenon arc lamp (Edison, NJ), which gave values of 0.273 (488 nm), 0.267 (523 nm), and 0.328 (568 nm).

Time-resolved delayed fluorescence and phosphorescence

Time-resolved delayed fluorescence and phosphorescence measurements were performed on an instrument similar to that described by Cobb et al. (1993). Excitation at 523 nm was provided by a TFR-523Q (Spectra-Physics) pulsed laser (~7-ns pulse width). The beam was routed through neutral density filters, an excitation polarizer, and, optionally, a half-wave plate used during g-factor determination. The emission was detected with right-angle geometry (L-format) through a saturated $K_2Cr_2O_7$ solution filter, an emission polarizer, and either a 515–565-nm bandpass (delayed fluorescence) or a 700-nm long-pass (phosphorescence) filter. The emission photons were collected via a Hamamatsu R928 photomultiplier tube (PMT) in single photon counting mode, housed in a Hamamatsu C1392–08 gated photomultiplier tube base. The gate width and delay were controlled by a Tennelec (Oak Ridge, TN) gate and delay generator, and an external signal generator was used as a trigger source for both the laser and detection electronics. The PMT signal was amplified by a Stanford Research Systems SR445 300 mHz amplifier and passed to a Stanford Research Systems SR430 multichannel scalar, and data were stored on a controlling DOS-compatible computer. Triggering was set at 70 Hz to allow EMA-band 3 emission to decay to background and the multichannel scalar to cycle. At experimental settings, the PMT was gated 215 ns after the multichannel scalar began collecting, and the laser pulse occurred 175 ns into the gate period. At minimum gate time, the PMT fully recovered by 1 μs after the laser pulse. Data were collected in 15,360 bins (640 ns wide; total decay time recorded was 9.83 ms). Prompt fluorescence emission arising from the trailing edge of the sharp excitation pulse was detected at early times, which contaminated the delayed fluorescence anisotropy data before ~20 μs. In the phosphorescence experiments, the time resolution was limited to ~5 μs by a small amount of prompt fluorescence contamination, which was absent in experiments that used a monochrometer to select wavelengths of ~715–745 nm (data not shown). The sample temperature was set and maintained by running water from a refrigerating/heating water bath through the water jacket of the cuvette holder.

Samples were purged of molecular oxygen using procedures described previously (Cobb et al., 1993). Erythrocyte ghost samples, prepared by the addition of 50 μl of eosin-labeled packed ghosts to 3 ml 5P7.4 (which contained 5 μg/ml PMSF), were equilibrated to 37° for 15 min in the sample chamber before data collection. No decrease in signal intensity was observed during the collection; separate decays were recorded every 25 min to verify data stability and were added together after collection. Anisotropy (r) and total intensity (S) were calculated as described by Cobb et al. (1993). The correction factor h (Jovin and Vaz, 1989), which corrects $S(t)$ for a finite detection aperture, was estimated from our instrumental geometry to be 1.96. By using subroutines incorporated into a Marquardt-Levenberg least-squares analysis package (Beechem et al., 1991; Beechem, 1992; Bevington, 1969), data sets were fit to either an empirical model (Eq. 17) or a multiple-population URD model, in which each population is described by Eq. 15, and all populations have the same preexponential amplitudes.

RESULTS

Orientation of a model system

Experimental verification of NA effects and their correction was provided by measurements on solutions of known anisotropy while varying the NA of the objective (data not shown). Erythrocyte membranes labeled with DiI were analyzed to test the orientation model developed in this work. In artificial membranes, the long axis of DiI has been reported to lie approximately perpendicular to the membrane normal axis (Badley et al., 1973; Timbs and Thompson, 1990, 1993), and in DiI-labeled human erythrocytes, a polarized fluorescence, wide-field microscopic approach yielded an orientation estimate of $\theta_a = 62°$, $\theta_e = 90°$, including a randomly oriented fraction of 0.15 (Axelrod, 1979); these values correspond to $\langle P_2(\cos\theta_a)\rangle = -0.14$, $\langle P_2(\cos\theta_e)\rangle = -0.43$. Shown in Fig. 3 are confocal microscopic data from DiI-labeled erythrocytes, and fits using model A, which yield orientation parameters for the DiI fluorescence transition dipoles (e.g., $\langle P_2(\cos\theta_a)\rangle = -0.28$, $\langle P_2(\cos\theta_e)\rangle = -0.44$). Fit parameters were constrained (Eq. 14) by using the steady-state anisotropy of 0.19 (data not shown). Considering the uncertainties about a randomly oriented fraction (Axelrod, 1979) and a collective lipid tilt and/or wobbling motion (discussed in Timbs and Thompson, 1993), there is clearly reasonable agreement with the previous studies.

Confocal microscopy and orientation of eosin covalently reacted with band 3

Shown in Fig. 4, *A* and *B*, are a sample polarized image pair of an eosin-labeled erythrocyte ghost membrane, demonstrating the intensity pattern that varies with the membrane tilt angle β. To exhibit this capping pattern, EMA must adopt a nonrandom orientation distribution when reacted with band 3. Because the intensity pattern has maxima at $\beta = 0°$ and 180° when excitation and emission polarizations are parallel (Fig. 4 *A*; compare to Fig. 2), it is expected that the absorption and emission dipole orientations are closer to 90° (perpendicular to the membrane normal axis) than to 0°

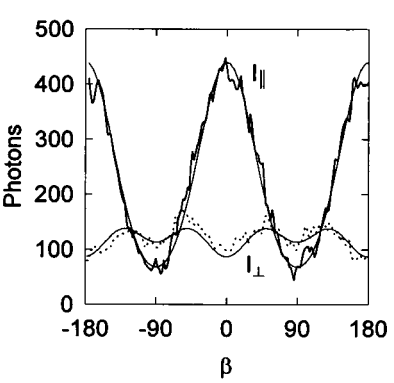

FIGURE 3 Orientation-dependent fluorescence intensities from 3 DiI-labeled erythrocyte ghosts at 20°C, and best-fit simulations. Shown are data collected using parallel (——) and perpendicular (·····) polarizer orientations. Fit was obtained using $\langle P_2(\cos\theta_a)\rangle = -0.284$ [−0.305, −0.262], $\langle P_2(\cos\theta_e)\rangle = -0.443$ [−0.477, −0.408], $\bar{C}_0 = 0.071$ [0.061, 0.081], $\bar{C}_1 = 0.063$ [0.049, 0.077], $\bar{C}_2 = 0.056$ [0.041, 0.072], where brackets denote 68% confidence intervals.

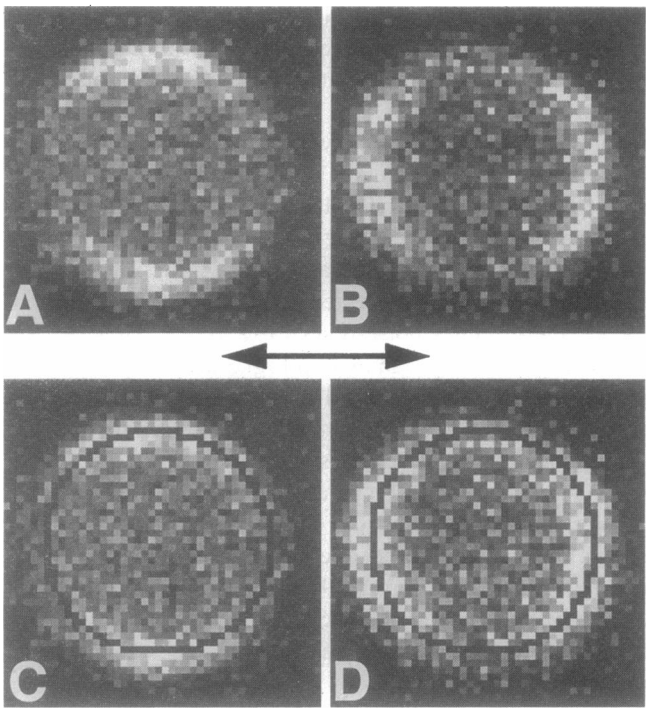

FIGURE 4 Polarized fluorescence images of a single EMA-labeled erythrocyte ghost at 20°C. Excitation polarization direction was horizontal, as denoted by arrows, and β is equal to 0 at the top of the membrane. Images were obtained using polarizer orientations parallel (*A*) and perpendicular (*B*) to the excitation. (*C* and *D*) Best-fit ellipse overlaid on the parallel (*C*) and perpendicular (*D*) polarized fluorescence images. Scale is 1 pixel = 0.2083 μm.

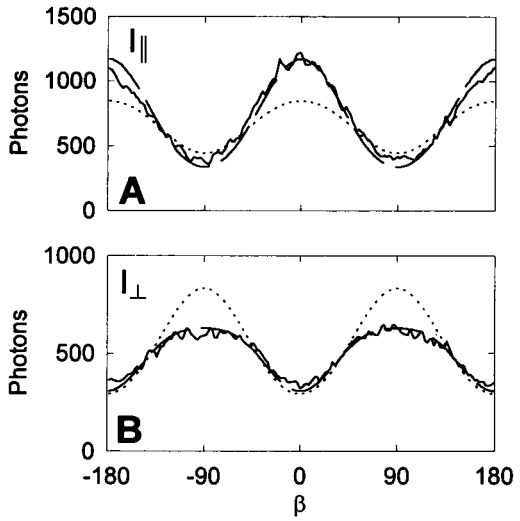

FIGURE 5 Orientation-dependent fluorescence intensity from 125 EMA-labeled erythrocyte ghosts (——) and the best-fit simulation (– – –). (*A*) Parallel polarizer orientation; (*B*) perpendicular. Fit to model A (simultaneous fit to parallel and perpendicular emission intensities) was obtained by using $\langle P_2(\cos\theta_a)\rangle = -0.096$ [−0.134, −0.056], $\langle P_2(\cos\theta_e)\rangle = -0.292$ [−0.340, −0.241], $\bar{C}_0 = 0.017$ [0.001, 0.033], $\bar{C}_1 = 0.047$ [0.025, 0.068], $\bar{C}_2 = 0.209$ [0.185, 0.234], where brackets denote 68% confidence intervals. For display, data was signal-averaged after baseline interpolation. For comparison with results from reconstituted band 3 (see Discussion), dotted lines (· · · ·) represent the best-fit simulation if the parameter θ_a is constrained to be 50°, $\langle P_2(\cos\theta_a)\rangle = 0.12$. Best-fit χ^2 is 1.13, which is significantly above the 95% confidence level for the unconstrained fit.

(parallel to the membrane normal). The data from the membrane border pixels (ellipse shown in Fig. 4, *C* and *D*) were adequately fit to model A ($\chi^2 = 0.992$), as shown in Fig. 5 (*solid lines*). Because of the low signal-to-noise ratio, it was necessary to simultaneously analyze data from 125 ghost membranes. The model's parameters contain orientational information ($\langle P_2(\cos\theta_a)\rangle$ and $\langle P_2(\cos\theta_e)\rangle$) and a combination of dynamics and orientation ($\bar{C}_0$, $\bar{C}_1$, $\bar{C}_2$). When the five parameters were freely varied, the data were adequately fit by a range of parameter values, all at identical values of χ^2. After constraining the correlation functions $\bar{C}_0$, $\bar{C}_1$, and $\bar{C}_2$ according to Eq. 14 ($\bar{r} = 0.273$), unique solutions were found. The order parameters $\langle P_2(\cos\theta_a)\rangle = -0.096$ and $\langle P_2(\cos\theta_e)\rangle = -0.292$ indicate that the absorption and emission dipoles of EMA are, on average, oriented at an angle greater than 54.7° to the membrane normal axis. The predicted r_∞ for uniaxial rotational diffusion (Eq. 16) is 0.011, which is similar in magnitude to the apparent r_∞ observed in time-resolved anisotropy measurements on trypsin-treated ghosts. The ratio $\bar{C}_2/\bar{C}_1$, which will be used as one approximation for $C_2(\infty)/C_1(\infty)$, is 4.5. This result indicates that, when the rotational diffusion of band 3 is modeled as URD, the e^{-4Dt} term makes the greatest contribution to the anisotropy decays. Data obtained at 10°C and 34°C had essentially identical fit parameters (not shown).

It is instructive to consider what kinds of orientation distributions could give rise to the five parameters observed in this fit to model A. A single fixed chromophore orientation was found not to fit the data well, which is not surprising, because EMA has a restricted-amplitude independent motion (see below). However, a good fit was obtained by assuming a Gaussian distribution of orientations (model B) and calculating the order parameters and correlation functions from that distribution ($\chi^2 = 0.992$; fit not shown). In this fit, the interdipole angle, θ_{ae}, was constrained to be 24° (based on time-resolved fluorescence anisotropy measurements, below), and the best-fit values were $\theta_a = 65°$, $\Delta\theta_a = 23°$, $\phi_{ae} = 0°$, and $\Delta\phi_{ae} = 0°$, although the fit was relatively insensitive to the values of ϕ_{ae} and $\Delta\phi_{ae}$ between 0° and 50°. Although the actual orientation distribution of EMA may be more complicated than a symmetric Gaussian distribution, this analysis shows that the order parameters and correlation functions found above can be derived from at least one physically reasonable orientation distribution.

Orientation studies on trypsin-treated ghosts

Mild trypsin treatment of erythrocyte ghosts has been shown to produce significant changes in the transient dichroism (Nigg and Cherry, 1980) and phosphorescence anisotropy decays, including a reduction in the apparent r_∞ (Matayoshi and Jovin, 1991). Trypsin-treated ghosts were

smaller than untreated ghosts (average diameter 5.1 ± 0.4 μm), and some fluorescent debris was visible in the microscope field. However, trypsin treatment produced no significant change in the confocal microscope data or the best-fit parameters (Fig. 6 *A*). This is also demonstrated by the rigorous confidence intervals shown in Fig. 6 *B* for the predicted fluorescence r_∞ calculated from Eq. 16 for trypsin-treated (*dashed lines*) and untreated (*solid lines*) ghosts.

Measurement of independent probe motion and estimation of the URD model preexponential amplitudes

The correlation functions $\bar{C}_0$, $\bar{C}_1$, and $\bar{C}_2$ depend on the rates and amplitudes of the independent dynamics of EMA on band 3, which have been measured with time-resolved prompt fluorescence anisotropy. Fig. 7 *A* shows the normalized time-resolved total intensity decay for EMA-band 3, without correcting for the ~100-ps scattering artifact. As demonstrated in Fig. 7 *B* (*upper curve*), the fluorescence anisotropy data are adequately fit by a single exponential decay component of 2.9 ns, with an apparent r_0 of 0.36 and r_∞ of 0.27. This motion is too slow for a freely mobile probe (e.g., free EMA in solution; Fig. 7 *B, lower curve*) but is appropriate for a limited-amplitude protein segmental motion (compare to Bicknese et al., 1995). Identical results were obtained for trypsin-treated EMA-labeled ghosts (data not shown).

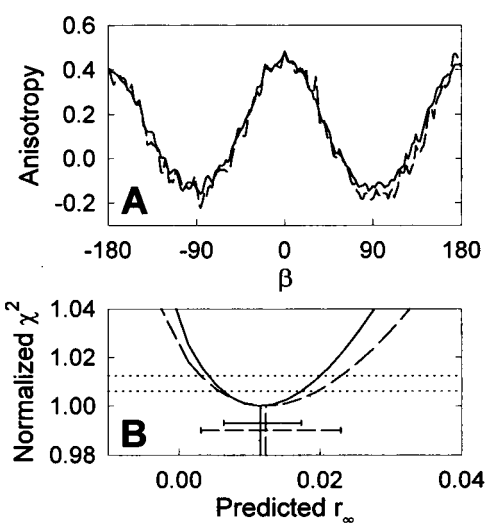

FIGURE 6 Effect of trypsin treatment on EMA orientation. (*A*) Comparison of orientation-dependent fluorescence anisotropy data from 125 EMA-labeled erythrocyte ghosts (——, same data as in Fig. 5), and 30 trypsin-treated EMA-labeled ghosts (– – –). For display, data was signal-averaged after baseline interpolation (see Materials and Methods). Best-fit parameters to model A (fit not shown) obtained for trypsin-treated ghosts were $\langle P_2(\cos\theta_a)\rangle = -0.097$ [−0.163, −0.025], $\langle P_2(\cos\theta_e)\rangle = -0.317$ [−0.401, −0.226], $\bar{C}_0 = 0.023$ [−0.008, 0.051], $\bar{C}_1 = 0.047$ [0.008, 0.084], $\bar{C}_2 = 0.204$ [0.161, 0.250], where brackets denote 68% confidence intervals. (*B*) Confidence interval plot for r_∞ as predicted by the URD model (Eq. 16), with error bars calculated from 68% confidence levels (·····). Best-fit values of this r_∞ are 0.011 [0.006, 0.017] (control, ——) and 0.012 [0.003, 0.022] (trypsin-treated, – – –).

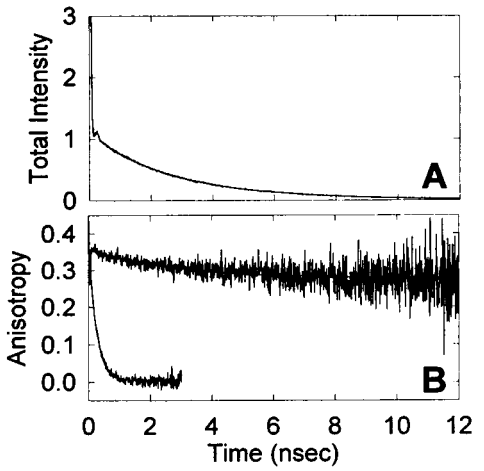

FIGURE 7 Time-resolved fluorescence anisotropy of EMA-labeled erythrocyte ghosts at 20°C. (*A*) The fluorescence intensity decay contained a fast scattering spike, which was subtracted using unlabeled ghost samples. Lifetimes were adequately fit by two exponential decays of characteristic time 1.39 ns (amplitude 21%) and 2.96 ns (amplitude 79%). (*B*) Background-subtracted fluorescence anisotropy data (*upper curve*) were adequately fit by the equation $r(t) = 0.089\exp(-t/2.9\text{ ns}) + 0.271$. (*Lower curve*) Fluorescence anisotropy decay recorded for free EMA in solution, fit by a single anisotropy decay component of 0.2 ns.

Because there is a limited amplitude motion during the fluorescence lifetime, the correlation functions reported by confocal microscopy (above) represent weighted averages over this motional process. As discussed in the Theory section, the preexponential amplitudes of the URD model correspond to the values after the motion has completely averaged the orientation distribution, $C_0(\infty)$, $C_1(\infty)$, and $C_2(\infty)$. Two approaches were taken to estimate these values from their time-averaged counterparts. First, without making assumptions about the form of the orientation distribution, the values were estimated from the r_∞ of the time-resolved fluorescence anisotropy. The anisotropy data were scaled (see Materials and Methods, above) to obtain a predicted r_0 at 488 nm of 0.300 (which is approximately consistent with the 22° interdipole angle found in Van der Heide et al., 1992) and a predicted r_∞ of 0.226. By using the procedure described above (Theory section), the amplitudes for the URD model were determined to be $C_0(\infty) = 0.011$, $C_1(\infty) = 0.039$, and $C_2(\infty) = 0.175$. A second method of estimating the URD amplitudes uses the functional form of the EMA orientation distribution, approximated as a Gaussian distribution (model B, above). The amplitude parameters may be calculated from that distribution and are $C_0(\infty) = 0.011$, $C_1(\infty) = 0.005$, and $C_2(\infty) = 0.190$. Although the resulting numbers differ in the two approaches, in both cases $C_2(\infty)$, which corresponds to the e^{-4Dt} decay component in the URD model, dominates the delayed fluorescence anisotropy decays.

Microsecond to millisecond rotational dynamics analyzed using known URD amplitudes

The time-resolved delayed fluorescence anisotropy decay of EMA-labeled erythrocyte ghosts, representing the micro-

second to millisecond rotational dynamics of band 3, is shown in Fig. 8. From Eq. 17, three exponential decay components were required to adequately fit the data (χ^2 = 0.982; fit not shown), and the apparent r_∞ is 0.066. Trypsin treatment produced a marked change in the delayed fluorescence anisotropy decay data and fit parameters (χ^2 = 0.985, fit not shown), and the apparent r_∞ decreased to 0.035. Fits to a multiple-oligomer URD model (based on Eq. 15), using the amplitudes determined in this work, required three URD populations and one immobile population (χ^2 = 0.985, control, *solid line*; χ^2 = 0.986, trypsin, *dashed line*). The good fits at early times support the assumption that the prompt fluorescence anisotropy reports all significant submicrosecond motions. The fastest populations in both samples are approximately consistent with freely rotating band 3 dimers or tetramers ($\tau = 1/6D$ = 16 μs (control) or 19 μs (trypsin-treated)).

By using the instrumentation described, earlier time resolutions and higher signal-to-noise ratios were obtained in phosphorescence anisotropy decay experiments. Although the orientation of the phosphorescence emission dipole remains unknown, according to the working model of multiple URD populations, the phosphorescence anisotropy should report identical decay times, which enables simultaneous analysis of the two data sets. Phosphorescence anisotropy decays of control and trypsin-treated (Fig. 9, *A* and *D*, respectively; *dashed lines*) ghosts were qualitatively similar to the delayed fluorescence anisotropy data presented here and those in previous reports (Matayoshi and Jovin, 1991). At 523 nm excitation, the delayed fluorescence anisotropy was numerically greater than the phosphorescence anisotropy, in contrast to the result obtained with 385-nm excitation (Matayoshi and Jovin, 1991). For each experimental treatment (control and trypsin-treated), the phosphorescence (*dashed lines*) and delayed fluorescence (*solid lines* and *dots*) anisotropy decays were simultaneously analyzed with the constraint that identical diffusion constants be used, whereas preexponential amplitudes were allowed to differ. The amplitudes for delayed fluorescence were fixed at $C_0(\infty)$ = 0.011, $C_1(\infty)$ = 0.039, and $C_2(\infty)$ = 0.175, as determined above. For each sample, three URD and one immobile population must be invoked to obtain a flat residual curve over the entire time range. As before, the fastest populations in each sample are approximately consistent with freely rotating band 3 dimers or tetramers ($\tau = 1/6D$ = 6.5 μs (control) or 19 μs (trypsin-treated)).

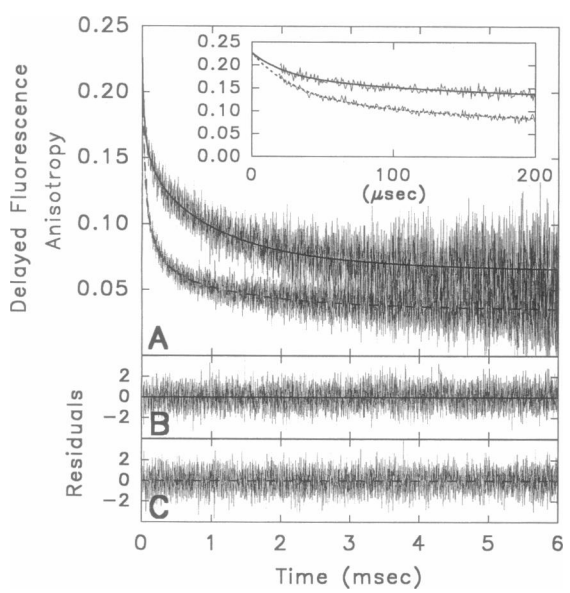

FIGURE 8 Overlaid are (*A*) delayed fluorescence anisotropy data and fits for EMA-labeled erythrocyte ghosts (upper decay fit is solid line), and for trypsin-treated ghosts (lower decay fit is dashed line). (*A, inset*) The first 200 μs of data and fits. (*B*) Residual ((data − fit)/variance) for control ghosts. (*C*) Residual for trypsin-treated ghosts. For clarity, every other data point is plotted, except in the inset, where every data point is plotted. Each decay represents 1 h of data collection. Fit parameters to the multiple-population URD model using the known EMA orientation are: control (χ^2 = 0.985), 16 μs (30%), 113 μs (11%), 683 μs (35%), immobile (24%); and trypsin (χ^2 = 0.986), 19 μs (53%), 131 μs (23%), 921 μs (13%), immobile (10%). Fit results using a sum of exponential decay components (Eq. 17, fits not shown) are: control (χ^2 = 0.982), decay constants 19 μs, 149 μs, 1214 μs, amplitudes 0.067, 0.035, 0.074, respectively, and r_∞ = 0.066; trypsin (χ^2 = 0.985), 35 μs, 196 μs, 1457 μs, amplitudes 0.092, 0.056, 0.033, respectively, and r_∞ = 0.035.

DISCUSSION

Optical spectroscopic measurements of the rotational diffusion of human erythrocyte band 3 have indicated multiple motional processes. However, correlation of these processes with actual molecular species has proved difficult. According to the URD model, the orientation of the optical probe eosin-5-maleimide on band 3 is expected to play a major role in the observed anisotropy decays. To facilitate analysis of optical data by the URD model, we have measured the orientation of eosin relative to the membrane normal axis. Analysis of anisotropy data using the measured orientation shows that the rotational rate of the fastest population is consistent with a band 3 dimer or tetramer, but that uncertainties remain about the true nature and source of the slower motions.

Complexities of band 3 rotational dynamics

Multiple exponential decays have been observed in the microsecond to millisecond optical anisotropy data for eosin-labeled band 3 in a number of independent studies (e.g., Nigg and Cherry, 1980; Tsuji et al., 1988; Matayoshi and Jovin, 1991; McPherson et al., 1992). These decays have been attributed to a heterogeneous mix of oligomers undergoing URD and/or to constraints on rotational diffusion imposed by interactions of the cytoplasmic domain of band 3 with the erythrocyte cytoskeleton. Consideration of the wealth of biochemical and ultrastructural data that have been reported in the literature over the past two decades should serve as the starting point for understanding the molecular bases for the various decay components (see

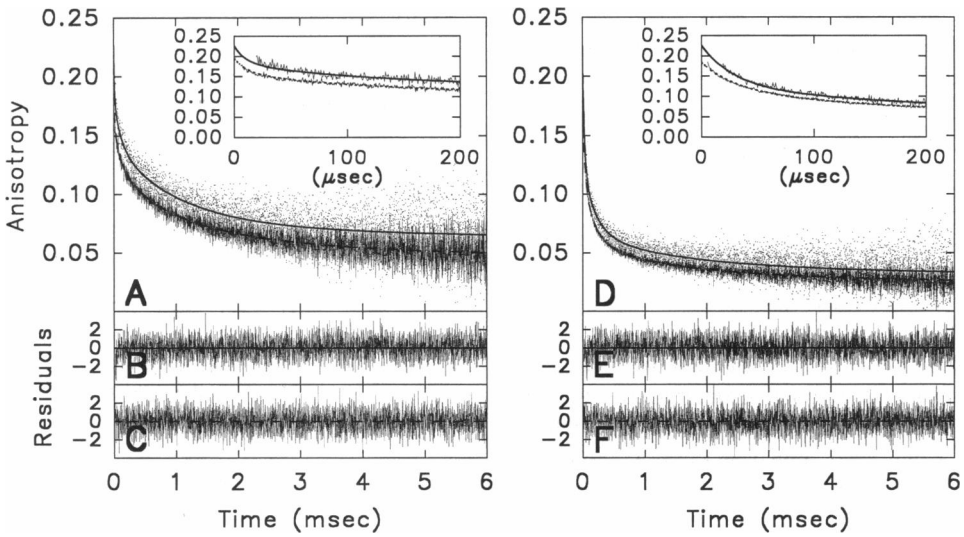

FIGURE 9 Simultaneous fits of delayed fluorescence and phosphorescence anisotropy data. (*A*) EMA-labeled control ghosts: delayed fluorescence (replot of Fig. 8 data, data are *dots*, fit is *solid line*) and phosphorescence anisotropy (lower decay, fit is *dashed line*). (*A, inset*) The first 200 μs of data and fits. (*B* and *C*) Residuals for control ghosts: phosphorescence and delayed fluorescence fits, respectively. (*D*) Trypsin-treated ghosts: delayed fluorescence (replot of Fig. 8 data, data are *dots*, fit is *solid line*) and phosphorescence anisotropy (lower decay, fit is *dashed line*). (*D, inset*) The first 200 μs of data and fits. (*E* and *F*) Residuals for trypsin-treated ghosts: phosphorescence and delayed fluorescence fits, respectively. For clarity, every other data point is plotted, except in the insets, where every data point is plotted. Each decay represents 1 h of data collection. Simultaneous fit parameters to the multiple-population URD model for delayed fluorescence (orientation known) and phosphorescence (orientation unknown) are: control (χ^2 = 1.006), 6.5 μs (22%), 78 μs (19%), 704 μs (35%), immobile (24%), phosphorescence amplitudes C_0 = −0.003, C_1 = 0.070, C_2 = 0.128; and trypsin (χ^2 = 0.995), 19 μs (55%), 158 μs (24%), 1440 μs (13%), immobile (9%), phosphorescence C_0 = 0.006, C_1 = 0.070, C_2 = 0.109. Fit results for phosphorescence anisotropy data using a sum of exponential decay components (Eq. 17, fits not shown) are: control (χ^2 = 1.010), decay constants 55 μs, 441 μs, 2136 μs, amplitudes 0.033, 0.039, 0.050, respectively, and r_∞ = 0.047; and trypsin (χ^2 = 0.992), 39 μs, 212 μs, 2143 μs, amplitudes 0.069, 0.053, 0.031, respectively, and r_∞ = 0.024.

Jennings, 1984; Low, 1986; Salhany, 1990; Wang, 1994; for representative reviews). First, the number of copies of band 3 monomer exceeds the apparent number of copies of ankyrin, the protein that mediates the link to the cytoskeleton, by approximately an order of magnitude (Steck, 1974; Bennett and Stenbuck, 1979). Thus, it is expected that at least a subpopulation of band 3 should exhibit rotational diffusion characterized by the size and shape of the transmembrane domain of the predominant stable oligomer. Second, a population is expected to be restricted in its rotational diffusion via interaction of the cytoplasmic domain with the cytoskeleton (reviewed in Low, 1986). The nature of this restriction could range from complete immobilization of the transmembrane domain if the linkage is rigid, to a restriction in amplitude of rotational motion with a flexible linkage, the latter case being suggested in a number of studies (reviewed in Wang, 1994). Third, even though studies have demonstrated that the dimer of band 3 is likely to be the fundamental unit (e.g., Staros and Kakkad, 1983; Wang et al., 1993, 1994), evidence has been presented for the existence of tetramers (e.g., Benz et al., 1984; Casey and Reithmeier, 1991) and possibly higher order aggregates (Rodgers and Glaser, 1993), although the latter interpretation appears to conflict with freeze-fracture electron microscopy results (Weinstein et al., 1980). The size of the rotating unit in the membrane can also be influenced by interactions between band 3 and other intrinsic membrane proteins, with glycophorin A being one candidate for such interactions (Che and Cherry, 1995). Finally, the possibility exists for limited amplitude off-axis rotations of band 3 and/or the eosin moiety, due to segmental motions within the protein or to interconversion of the distal xanthine moiety of eosin between different regions of the protein structure.

Despite this potential complexity, it should be emphasized that the first four situations described in the previous paragraph would be expected to lead to species whose rotational diffusion is dominated by motions about the membrane normal axis. As discussed further below and as described in Results, we have employed the restrictions placed upon the amplitudes and residual anisotropy from the microscope studies to address the question of how many URD species must be invoked to account for the observed anisotropy decays. Moreover, we have asked the pertinent question, which diffusion coefficients obtained from these analyses are consistent with the various expected molecular species described above?

Orientation model

We have developed a theoretical model to predict the angle-dependent polarized fluorescence emission, given two order parameters and three correlation functions of the fluorophore orientation distribution. Whereas microscopic polar-

ized fluorescence images of single cells have been used previously to determine chromophore orientation (Axelrod, 1979; Florine-Casteel, 1990), the models used in those studies make specific assumptions about the form of the nanosecond time scale motion that do not apply to eosin-labeled band 3. Other previous work provides examples of determination of transition dipole orientations by angle-dependent fluorescence measurements (e.g., Van der Meer et al., 1982; Van der Heide et al., 1994; Burghardt and Ajtai, 1994). However, the experimental geometries used to derive the previous models are not compatible with our instrument. Furthermore, where previous work expanded the correlation functions in terms of orientational order parameters, our primary interest was the values of the correlation functions themselves, because they also appear as the preexponential amplitudes of the URD model. Ultimately, the orientation measurements made by confocal microscopy have been used to constrain the URD model for dynamics measurements made in bulk solution.

Orientation of EMA on band 3

Good fits to the present confocal microscope data have been obtained with two orientation distribution models: one that makes no assumptions about the distribution but yields limited information about the distribution (model A), and one that approximates the orientation distribution as Gaussian (model B). This information may be compared to a number of biochemical and biophysical studies that offer insight into the nature of the EMA binding site. The covalent reaction site, Lys-430, is thought to lie in the first extracellular loop of the integral membrane domain of band 3 (Wang et al., 1994). However, the EMA chromophore appears to be bound within a protein pocket that is separated from the bulk solution (Pan and Cherry, 1995) and appears to lie deep within the membrane permeability barrier (Macara et al., 1983). The stilbenedisulfonate binding site, which is not identical to but is thought to overlap with the EMA binding site, also appears to lie in a pocket deep within the protein (Pimplikar and Reithmeier, 1986; Landolt-Marticorena et al., 1995; Rao et al., 1979), protected from solvent exposure (Scothorn et al., 1996). Whereas low-resolution structural information only hints at the location and disposition of these binding sites (Wang et al., 1994), we may make some reasonable guesses as to the orientation of the eosin chromophore. With the maleimide group reacted with Lys-430 at the extracellular surface, and the eosin chromophore bound deep within the transmembrane core of the protein, a reasonable orientation for the long axis of xanthine moiety would be approximately perpendicular to the membrane normal axis. This study shows that the emission dipole of EMA, which lies along the long axis of the xanthine moiety (Van der Heide et al., 1992), is approximately perpendicular to the membrane normal axis, consistent with this rough orientation model.

Exponential decay components of the URD model

The URD model approximates membrane protein rotational dynamics as uniaxial rotation about the membrane normal axis (Saffman and Delbrück, 1975; Jähnig, 1986). Written explicitly for fixed-orientation absorption and emission dipoles (see Fig. 1 *B*), the time-resolved anisotropy predicted by the URD model (Eq. 15) becomes

$$r(t) = C_0 + C_1 e^{-Dt} + C_2 e^{-4Dt}$$

$$C_0 = \frac{1}{10}(3\cos^2\theta_a - 1)(3\cos^2\theta_e - 1)$$

$$C_1 = \frac{6}{5}\sin\theta_a \cos\theta_a \sin\theta_e \cos\theta_e \cos\Psi \tag{18}$$

$$C_2 = \frac{3}{10}\sin^2\theta_a \sin^2\theta_e \cos 2\Psi.$$

The finding that the preexponential amplitude C_2 is much larger than C_1 (and that C_1 may in fact be negligible) is very important for interpreting the time-resolved anisotropy decays of band 3. According to this result, the URD model predicts that anisotropy decays for EMA band 3 are dominated by the e^{-4Dt} decay term instead of the e^{-Dt} term. Calculations performed assuming the orientation distribution is Gaussian predict that this result should be true for phosphorescence anisotropy decays as well. On the other hand, fluorescence depletion experiments (Johnson and Garland, 1981) suggested that the e^{-Dt} term was significant. However, potential difficulties with probe labeling and experimental setup in the previous study (discussed in Wegener, 1984; and Hellen and Burghardt, 1994) make it difficult to compare those results with the current work.

Comparison of the orientational r_∞ with values observed in time-resolved anisotropy experiments

If band 3 motion is modeled as URD, the orientation results in this study offer a prediction of the residual anisotropy (r_∞). Because prompt and delayed fluorescence utilize the same transition dipole moments, this predicted r_∞ may be directly compared to the value observed in a delayed fluorescence experiment. The r_∞ predicted from microscopy data is 0.011 (68% confidence interval of [0.006, 0.017]). In contrast, the delayed fluorescence anisotropy of eosin-labeled ghosts reaches an apparent r_∞ of 0.066 in 10 ms. This suggests that rotational motion is hindered in some way, such as the amplitude of rotational diffusion is constrained by interaction with cytoskeletal proteins, or a population of band 3 exists in aggregates that are immobile on this time scale. However, if we assume that the radius of a band 3 aggregate increases approximately as the square root of the number of monomers involved and take the confocal r_∞ of

0.011 to represent the r_∞ in the absence of aggregation, this result would require that about 25% of band 3 be present in the form of aggregates that are immobile on a 10-ms time scale (≥5000 copies per aggregate).

Anisotropy decays of trypsin-treated ghosts are significantly different from controls (Nigg and Cherry, 1980). In the present work we have shown that the orientation of eosin and the predicted uniaxial r_∞ are not altered by trypsin treatment, which indicates that the changes in anisotropy decays represent a dynamic rather than orientational process. This also suggests that the motional processes between ~100 μs and ~10 ms, which are significantly altered by trypsin treatment, do not perturb C_0, C_1, and C_2 and are dominated by motions about the membrane normal axis. The delayed fluorescence r_∞ of trypsin-treated ghosts is 0.035, which is on the same order of magnitude, but is larger than the predicted r_∞. Assuming that this difference is significant, two possibilities are suggested: first, hindrance to uniaxial motion (such as through oligomerization or association with the cytoskeleton) may remain, even in trypsin-treated ghosts, or second, motions outside the measurement windows might contribute to the orientation distribution (reducing the predicted r_∞) without affecting time-resolved measurements.

The orientation measurements in this study can potentially be used to interpret transient dichroism data according to the URD model. Expressions for the preexponential amplitudes C_0, C_1, and C_2 may be obtained by replacing θ_e in Eq. 18 with θ_a, and setting $\psi = 0$. First, the predicted r_∞, or C_0, is given by $2/5\ \langle P_2(\cos\theta_a)\rangle^2$. Second, examination of the trigonometric form of the equations reveals that for this special case, $C_2 = (1 - \langle P_2(\cos\theta_a)\rangle^2/6$. Third, C_1 is determined by the difference in r_o and the sum $C_0 + C_2$ (Eq. 14). Assuming that the amount of fast depolarization of dichroism is equal to that observed for fluorescence in this study (0.27/0.36), the predicted r_o for transient dichroism is 0.3. This determines the three amplitudes C_0, C_1, and C_2 to be 0.004, 0.096, and 0.200, respectively. As expected, these amplitudes are not consistent with any single fixed orientation of the eosin molecule, but are consistent with a limited-amplitude independent probe motion. As with delayed fluorescence anisotropy, C_2, the amplitude of the e^{-4Dt} decay term, is larger than C_1. These predicted preexponential amplitudes are reasonably consistent with a reported transient dichroism r_∞ of 0.02 at 2 ms (Morrison et al., 1986) and one of their two possible values of the angle between the absorption dipole and the membrane normal (66°). In contrast, a preliminary steady-state linear dichroism measurement on reconstituted eosin-labeled band 3 suggested that this angle between the absorption dipole and the membrane normal was 50° (Mühlebach, 1984). As that previous experiment used band 3 reconstituted into vesicles and flattened before absorption measurements, it is possible that artifacts were introduced at some point during the procedure. The orientation data shown in Fig. 5, with the fit obtained when the parameter θ_a is constrained to be 50° (*dotted lines*), demonstrate that the result obtained in erythrocyte ghost membranes is significantly different.

Uniaxial rotational diffusion constants for band 3 rotational dynamics

The complexity of band 3 optical spectroscopic data has prevented the assignment of exponential decay components to specific physical models. Although a model that postulates large quantities of band 3 aggregates is capable of describing the experimental data, independent verification of this model's predictions are still forthcoming. Nevertheless, we have attempted to answer two specific questions: Using the chromophore orientation results in this work, how many uniaxially rotating species are required to fit the experimental data, and what are their rotational diffusion constants?

It is useful first to estimate the rotational diffusion constant of a band 3 dimer, which is given by (Saffman and Delbrück, 1975)

$$D_\parallel = \frac{kT}{4\pi\eta r^2 h}, \tag{19}$$

where η is the membrane effective viscosity, h is the membrane thickness, and r is the effective radius of the intramembrane portion of band 3. Different values have been reported for the effective membrane viscosity, with a value of 1 poise appearing to be a reasonable estimate at 37°C, and low-resolution crystal structures indicate an average radius of a band 3 dimer of ~55 Å (Wang et al., 1994). From these figures, a rough estimate for the rotational diffusion constant at 37°C for a band 3 dimer is 23,500 s^{-1}, which corresponds to a rotational correlation time (defined as $\tau = 1/6D$) of 7 μs.

Delayed fluorescence anisotropy data were obtained for trypsin-treated and untreated erythrocyte ghost samples at 37°C. Fits to an empirical sum-of-exponentials model (Eq. 17) show a spread in decay constants over three orders of magnitude, similar to previous results obtained from transient dichroism and phosphorescence anisotropy. Reanalysis of these data using a multiple-population URD model (based on Eq. 15) required three URD and one immobile population for adequate fits. The rotational correlation times ($1/6D_\parallel$) for the fastest component in each sample are 16 and 19 μs for control and trypsin-treated ghosts. When the phosphorescence anisotropy data, which have greater signal-to-noise and a earlier time resolution but an unknown emission dipole orientation, are included in this analysis, the fastest correlation times are 7 and 19 μs for control and trypsin-treated ghosts. Within the uncertainties outlined above, these values are consistent with freely rotating band 3 dimers or tetramers. Furthermore, as with previous optical spectroscopic results, this analysis according to multiple populations might be taken to suggest that 50–70% of band 3 is aggregated to some degree. Other potential sources of the slower decays have been discussed above.

Comparison of rotational correlation times and ST-EPR results

Recent studies by Hustedt and Beth (1995), using a newly developed spin-labeled stilbenedisulfonate as an affinity probe, have indicated that the rotational diffusion of band 3 in ghost membranes can be adequately described by a URD model with a correlation time of 8 μs. This result is remarkably consistent with the fastest decay time observed in the current studies. However, fitting of the ST-EPR data did not require the inclusion of a major fraction of slowly rotating or immobile species. In fact, when such a two-component model was tested, the nonlinear least-squares fitting converged to a single uniaxial species (Hustedt and Beth, 1995). The authors discussed several potential explanations for different sensitivities of optical anisotropy and ST-EPR to very slow and to constrained diffusion models. Although most of this discussion will not be repeated here, it is worth reemphasizing that the ST-EPR work strongly suggested that most, if not all, of the copies of band 3 present were undergoing rotational motion, of relatively large amplitude, in the 8-μs time window. Therefore, one must consider the possibility that the fastest decay observed in these studies arises from a motional mode common to most of the copies of band 3 present, and that the additional longer decays represent other motional processes that occur on a slower time scale.

Much work remains to be done to rigorously assign the various decay components to molecular species present and potentially build a unifying model that is consistent with optical, ST-EPR, and biochemical data. One approach that deserves serious attention is the expression of band 3, including mutants lacking the cytoplasmic domain, in other cell types in which one might hope to have some control over the number of copies of protein expressed on the cell surface. The comparison of ST-EPR and optical anisotropy data from such a system would undoubtedly add substantially to our current understanding of the nature and extent of the interactions between band 3 and other proteins of the erythrocyte membrane.

The authors wish to thank Dr. J. M. Beechem for his assistance in performing the time-resolved prompt fluorescence anisotropy experiments, Dr. E. J. Hustedt for his assistance with the nonlinear least-squares analysis, Dr. R. A. Stein for helpful discussions, and Dr. B. W. van der Meer for critically reading the manuscript.

This work was supported by a grant from the National Institutes of Health to AHB (HL 34737) and utilized equipment in the Vanderbilt Medical Center Cell Imaging Shared Resource. DWP is a Beckman Young Investigator of the Arnold and Mabel Beckman Foundation. SMB is supported by National Institutes of Health training grant T32 GM07347.

REFERENCES

Axelrod, D. 1979. Carbocyanine dye orientation in red cell membrane studied by microscopic fluorescence polarization. *Biophys. J.* 26: 557–573.

Badley, R. A., W. G. Martin, and H. Schneider. 1973. Dynamic behavior of fluorescent probes in lipid bilayer model membranes. *Biochemistry.* 12:268–275.

Beechem, J. M. 1992. Global analysis of biochemical and biophysical data. *Methods Enzymol.* 210:37–54.

Beechem, J. M., E. Gratton, M. Ameloot, J. R. Knutson, and L. Brand. 1991. The global analysis of fluorescence intensity and anisotropy decay data: second generation theory and programs. *In* Topics in Fluorescence Spectroscopy, Vol. 2: Principles. J. R. Lakowicz, editor. Plenum Press, New York. 241–305.

Bennett, V., and P. J. Stenbuck. 1979. The membrane attachment protein for spectrin is associated with band 3 in human erythrocyte membranes. *Nature.* 280:468–473.

Benz, R., M. T. Tosteson, and D. Schubert. 1984. Formation and properties of tetramers of band 3 protein from human erythrocyte membranes in planar lipid bilayers. *Biochim. Biophys. Acta.* 775:347–55.

Beth, A. H., T. E. Conturo, S. D. Venkataramu, and J. V. Staros. 1986. Dynamics and interactions of the anion channel in intact human erythrocytes: an electron paramagnetic resonance spectroscopic study employing a new membrane-impermeant bifunctional spin-label. *Biochemistry.* 25:3824–3832.

Bevington, P. R. 1969. Data Reduction and Error Analysis for the Physical Sciences. McGraw-Hill, New York.

Bicknese, S., M. Rossi, B. Thevenin, S. B. Shohet, and A. S. Verkman. 1995. Anisotropy decay measurement of segmental dynamics of the anion binding domain in erythrocyte band 3. *Biochemistry.* 34: 10645–10651.

Blackman, S. M., E. J. Hustedt, A. H. Beth, and D. W. Piston. 1995. Orientation studies of the optical probe eosin-5-maleimide covalently bound to erythrocyte band 3 by confocal polarization microscopy. *Biophys. J.* 68:A291.

Blackman, S. M., E. J. Hustedt, C. E. Cobb, D. W. Piston, and A. H. Beth. 1996. Analysis of rotational diffusion measurements of eosin-5-maleimide-labeled band 3 in terms of the uniaxial rotational diffusion model. *Biophys. J.* 70:A331.

Burghardt, T. P., and K. Ajtai. 1994. Following the trajectory of the principal hydrodynamic frame of a protein using multiple probes. *Biochemistry.* 33:5376–5381.

Casey, J. R., and R. A. F. Reithmeier. 1991. Analysis of the oligomeric state of band 3, the anion transport protein of the human erythrocyte membrane, by size exclusion high performance liquid chromatography. Oligomeric stability and origin of heterogeneity. *J. Biol. Chem.* 266: 15726–15737.

Che, A., and R. J. Cherry. 1995. Loss of rotational mobility of band 3 proteins in human erythrocyte membranes induced by antibodies to glycophorin A. *Biophys. J.* 68:1881–1887.

Cherry, R. J., A. Burkli, M. Busslinger, G. Schneider, and G. R. Parish. 1976. Rotational diffusion of band 3 proteins in the human erythrocyte membrane. *Nature.* 263:389–393.

Cherry, R. J., and R. E. Godfrey. 1981. Anisotropic rotation of bacteriorhodopsin in lipid membranes. *Biophys. J.* 36:257–276.

Cobb, C. E., and A. H. Beth. 1990. Identification of the eosinyl-5-maleimide reaction site on the human erythrocyte anion-exchange protein: overlap with the reaction sites of other chemical probes. *Biochemistry.* 29:8283–8290.

Cobb, C. E., E. J. Hustedt, J. M. Beechem, and A. H. Beth. 1993. Protein rotational dynamics investigated with a dual EPR/optical molecular probe: spin-labeled eosin. *Biophys. J.* 64:605–613.

Corbett, J. D., and D. E. Golan. 1993. Band 3 and glycophorin are progressively aggregated in density-fractionated sickle and normal red blood cells. *J. Clin. Invest.* 91:208–217.

Dix, J. A., and A. S. Verkman. 1990. Mapping of fluorescence anisotropy in living cells by ratio imaging. Application to cytoplasmic viscosity. *Biophys. J.* 57:231–240.

Edmonds, A. R. 1960. Angular Momentum in Quantum Mechanics. Princeton University Press, Princeton, NJ.

Fairbanks, G., T. L. Steck, and D. F. H. Wallach. 1971. Electrophoretic analysis of the major polypeptides of the human erythrocyte membrane. *Biochemistry.* 10:2606–2617.

Florine-Casteel, K. 1990. Phospholipid order in gel- and fluid-phase cell-size liposomes measured by digitized video fluorescence polarization microscopy. *Biophys. J.* 57:1199–1215.

Hellen, E. H., and T. P. Burghardt. 1994. Saturation effects in polarized fluorescence photobleaching recovery and steady state fluorescence polarization. *Biophys. J.* 66:891–897.

Heyn, M. P., R. J. Cherry, and U. Müller. 1977. Transient and linear dichroism studies on bacteriorhodopsin: determination of the orientation of the 568 nm all-*trans* retinal chromophore. *J. Mol. Biol.* 117:607–620.

Hustedt, E. J., and A. H. Beth. 1995. Analysis of saturation-transfer electron paramagnetic resonance spectra of a spin-labeled integral membrane protein, band 3, in terms of the uniaxial rotational diffusion model. *Biophys. J.* 69:1409–1423.

Hustedt, E. J., and A. H. Beth. 1996. The determination of the orientation of a band 3 affinity spin-label relative to the membrane normal axis of the human erythrocyte. *Biochemistry.* In press.

Jähnig, F. 1986. The shape of a membrane protein derived from rotational diffusion. *Eur. Biophys. J.* 14:63–64.

Jennings, M. L. 1984. Oligomeric structure and the anion transport function of human erythrocyte band 3 protein. *Mol. Membr. Biol.* 80: 105–117.

Johnson, P., and P. B. Garland. 1981. Depolarization of fluorescence depletion: a microscopic method for measuring rotational diffusion of membrane proteins on the surface of a single cell. *FEBS Lett.* 132: 252–256.

Jovin, T. M., and W. L. C. Vaz. 1989. Rotational and translational diffusion in membranes measured by fluorescence and phosphorescence methods. *Methods Enzymol.* 172:471–513.

Laemmli, U. K. 1970. Cleavage of structural proteins during the assembly of the head of bacteriophage T4. *Nature.* 227:680–685.

Landolt-Marticorena, C., J. R. Casey, and R. A. F. Reithmeier. 1995. Transmembrane helix-helix interactions and accessibility of H_2DIDS on labelled band 3, the erythrocyte anion exchange protein. *Mol. Membr. Biol.* 12:173–182.

Lepke, S., and H. Passow. 1976. Effects of incorporated trypsin on anion exchange and membrane proteins in human red blood cell ghosts. *Biochim. Biophys. Acta.* 455:353–370.

Lieberman, D. M., and R. A. F. Reithmeier. 1988. Localization of the carboxyl terminus of band 3 to the cytoplasmic side of the erythrocyte membrane using antibodies against a synthetic peptide. *J. Biol. Chem.* 263:10022–10028.

Lin, S. W., and R. A. Mathies. 1989. Orientation of the protonated retinal Schiff base group in bacteriorhodopsin from absorption linear dichroism. *Biophys. J.* 56:653–660.

Low, P. S. 1986. Structure and function of the cytoplasmic domain of band 3: center of erythrocyte membrane-peripheral protein interactions. *Biochim. Biophys. Acta.* 864:145–167.

Lux, S. E., K. M. John, R. R. Kopito, H. F. Lodish. 1989. Cloning and characterization of band 3, the human erythrocyte anion-exchange protein (AE1). *Proc. Natl. Acad. Sci. USA.* 86:9089–9093.

Macara, I. G., S. Kuo, and L. C. Cantley. 1983. Evidence that inhibitors of anion exchange induce a transmembrane conformational change in band 3. *J. Biol. Chem.* 258:1785–1792.

Matayoshi, E. D., and T. M. Jovin. 1991. Rotational diffusion of band 3 in erythrocyte membranes. 1. Comparison of ghosts and intact cells. *Biochemistry.* 30:3527–3538.

Matayoshi, E. D., W. H. Sawyer, and T. M. Jovin. 1991. Rotational diffusion of band 3 in erythrocyte membranes. 2. Binding of cytoplasmic enzymes. *Biochemistry.* 30:3538–3543.

McPherson, R. A., W. H. Sawyer, and L. Tilley. 1992. Rotational diffusion of the erythrocyte integral membrane protein band 3: effect of hemichrome binding. *Biochemistry.* 31:512–518.

McPherson, R. A., W. H. Sawyer, and L. Tilley. 1993. Band 3 mobility in camelid elliptocytes: implications for erythrocyte shape. *Biochemistry.* 32:6696–6702.

Morrison, I. E. G., T. J. Mühlebach, and R. J. Cherry. 1986. Rotational diffusion of band 3 reconstituted into lipid vesicles: an application of global analysis. *Biochem. Soc. Trans.* 14:885–886.

Mühlebach, T. J. 1984. Investigation of the rotational diffusion and self-association of band 3 in the erythrocyte membrane and in reconstituted vesicles. Ph.D. thesis. Eidgenössiche Technische Hochschule, Zurich, Switzerland.

Nigg, E. A., and R. J. Cherry. 1980. Anchorage of a band 3 population at the erythrocyte cytoplasmic membrane surface: protein rotational diffusion measurements. *Proc. Natl. Acad. Sci. USA.* 77:4702–4706.

Palek, J., and S. Lambert. 1990. Genetics of the red cell membrane skeleton. *Semin. Hematol.* 27:290–332.

Pan, R. J., and R. J. Cherry. 1995. Evidence that eosin-5-maleimide binds close to the anion transport site of human erythrocyte band 3: a fluorescence quenching study. *Biochemistry.* 34:4880–4888.

Pimplikar, S. W., and R. A. F. Reithmeier. 1986. Affinity chromatography of band 3, the anion transport protein of erythrocyte membranes. *J. Biol. Chem.* 261:9770–9778.

Press, W. H., S. A. Teukolsky, W. T. Vetterling, and B. P. Flannery. 1992. Numerical Recipes in Fortran: The Art of Scientific Computing, 2nd Ed. Cambridge University Press, New York.

Rao, A., P. Martin, R. A. F. Reithmeier, and L. C. Cantley. 1979. Location of the stilbenedisulfonate binding site of the human erythrocyte anion-exchange system by resonance energy transfer. *Biochemistry.* 18: 4505–4516.

Rigler, R., and M. Ehrenberg. 1973. Molecular interactions and structure as analysed by fluorescence relaxation spectroscopy. *Q. Rev. Biophys.* 6:139–199.

Rodgers, W., and M. Glaser. 1993. Distributions of proteins and lipids in the erythrocyte membrane. *Biochemistry.* 32:12591–12598.

Saffman, P. G., and M. Delbrück. 1975. Brownian motion in biological membranes. *Proc. Natl. Acad. Sci. USA.* 72:3111–3113.

Salhany, J. M. 1990. Erythrocyte Band 3 Protein. CRC Press, Boca Raton, FL.

Sandison, D. R., D. W. Piston, R. M. Williams, and W. W. Webb. 1995. Quantitative comparison of background rejection, signal-to-noise ratio, and resolution in confocal and full-field laser scanning microscopes. *Appl. Optics.* 34:3576–3588.

Sandison, D. R., and W. W. Webb. 1994. Background rejection and signal-to-noise optimization in confocal and alternative fluorescence microscopes. *Appl. Optics.* 33:603–615.

Scothorn, D. S., W. E. Wojcicki, E. J. Hustedt, A. H. Beth, and C. E. Cobb. 1996. Synthesis and characterization of a novel spin-labeled affinity probe of human erythrocyte band 3: characteristics of the stilbenedisulfonate binding site. *Biochemistry.* In press.

Staros, J. V., and B. P. Kakkad. 1983. Cross-linking and chymotryptic digestion of the extracytoplasmic domain of the anion exchange channel in intact human erythrocytes. *J. Membr. Biol.* 74:247–254.

Steck, T. L. 1974. The organization of proteins in the human red blood cell membrane. A review. *J. Cell Biol.* 62:1–19.

Szabo, A. 1984. Theory of fluorescence depolarization in macromolecules and membranes. *J. Chem. Phys.* 81:150–167.

Tanner, M. J., P. G. Martin, and S. High. 1988. The complete amino acid sequence of the human erythrocyte membrane anion-transport protein deduced from the cDNA sequence. *Biochem. J.* 256:703–712.

Thomas, D. D. 1985. Saturation transfer EPR studies of microsecond rotational motions in biological membranes. *In* The Enzymes of Biological Membranes, Vol. 2, 2nd Ed. A. N. Martonosi, editor. Plenum Press, New York. 287–312.

Thomas, D. D. 1986. Rotational diffusion of membrane proteins. *In* Techniques for the Analysis of Membrane Proteins. C. I. Ragan and R. J. Cherry, editors. Chapman and Hall, London. 377–431.

Timbs, M. M., and N. L. Thompson. 1990. Slow rotational mobilities of antibodies and lipids associated with substrate-supported phospholipid monolayers as measured by polarized fluorescence photobleaching recovery. *Biophys. J.* 58:413–428.

Timbs, M. M., and N. L. Thompson. 1993. Measurement of restricted rotational diffusion of fluorescent lipids in supported planar phospholipid monolayers using angle-dependent polarized fluorescence photobleaching recovery. *Biopolymers.* 33:45–57.

Tsuji, A., K. Kawasaki, S. Ohnishi, H. Merkle, and A. Kusumi. 1988. Regulation of band 3 mobilities in erythrocyte ghost membranes by protein association and cytoskeletal meshwork. *Biochemistry.* 27: 7447–7452.

Van der Heide, U. A., B. Orbons, H. C. Gerritsen, and Y. K. Levine. 1992. The orientation of transition moments of dye molecules used in fluorescence studies of muscle systems. *Eur. Biophys. J.* 21:263–272.

Van der Heide, U. A., O. E. Rem, H. C. Gerritsen, E. L. de Beer, P. Schiereck, I. P. Trayer, and Y. K. Levine. 1994. A fluorescence depolarization study of the orientational distribution of cross-bridges in muscle fibres. *Eur. Biophys. J.* 23:369–378.

Van der Meer, W., R. H. P. Kooyman, and Y. K. Levine. 1982. A theory of fluorescence depolarization in macroscopically ordered membrane systems. *Chem. Phys.* 66:39–50.

Wang, D. N. 1994. Band 3 protein: structure, flexibility and function. *FEBS Lett.* 346:26–31.

Wang, D. N., W. Kühlbrandt, V. E. Sarabia, and R. A. F. Reithmeier. 1993. Two-dimensional structure of the membrane domain of human band 3, the anion transport protein of the erythrocyte membrane. *EMBO J.* 12:2233–2239.

Wang, D. N., V. E. Sarabia, R. A. F. Reithmeier, and W. Kühlbrandt. 1994. Three-dimensional map of the dimeric membrane domain of the human erythrocyte anion exchanger, band 3. *EMBO J.* 13:3230–3235.

Wegener, W. A. 1984. Fluorescence recovery spectroscopy as a probe of slow rotational motions. *Biophys. J.* 46:795–803.

Weinstein, R. S., J. K. Khodadad, and T. L. Steck. 1980. The band 3 protein intramembrane particle of the human red blood cell. *In* Membrane Transport in Erythrocytes. U. V. Llassen, H. H. Ussing, and J. O. Wieth, editors. Munksgaard, Copenhagen. 35–50.

Zannoni, C., A. Arcioni, and P. Cavatorta. 1983. Fluorescence depolarization in liquid crystals and membrane bilayers. *Chem. Phys. Lipids.* 32:179–250.